CHAPTER SIXTEEN

Two-Photon Microscopy and Multidimensional Analysis of Cell Dynamics

Bernd H. Zinselmeyer,[*] John Dempster,[†] David L. Wokosin,[‡] Jonathan J. Cannon,[§] Robert Pless,[§] Ian Parker,[¶] *and* Mark J. Miller[*]

Contents

[*] Washington University School of Medicine, Department of Pathology and Immunology, St. Louis, Missouri, USA
[†] University of Strathclyde, Institute for Pharmacy & Biomedical Sciences, Glasgow, Scotland, United Kingdom
[‡] Northwestern University, Department of Physiology, Chicago, Illinois, USA
[§] Department of Computer Science and Engineering, Washington University in St. Louis, St. Louis, Missouri, USA
[¶] Departments of Neurobiology and Behavior, and Physiology and Biophysics, University of California, Irvine, California, USA

Methods in Enzymology, Volume 461
ISSN 0076-6879, DOI: 10.1016/S0076-6879(09)05416-0

Abstract

Two-photon (2P) microscopy is a high-resolution imaging technique that was initially applied by neurobiologists and developmental cell biologists but has subsequently been broadly adapted by immunologists. The value of 2P microscopy is that it affords an unparalleled view of single-cell spatiotemporal dynamics deep within intact tissues and organs. As the technology develops and new transgenic mice and fluorescent probes become available, 2P microscopy will serve as an increasingly valuable tool for assessing cell function and probing molecular mechanisms. Here we discuss the technical aspects related to 2P microscope design, explain in detail various tissue imaging preparations, and walk the reader through the often daunting process of analyzing multidimensional data sets and presenting the experimental results.

1. Introduction

The theory describing two-photon (2P) excitation of fluorescence was first published by Maria Göppert (1929) as part of her doctoral work in physics at the University of Göttingen. Nearly 60 years later, Denk and Webb introduced 2P microscopy as a high-resolution imaging technique for studying biologic tissues (Denk *et al.*, 1990). Neurobiologists were among the first to adopt 2P microscopy for biologic studies (Yuste *et al.*, 2005), but it is now used widely by cell biologists and immunologists (Germain *et al.*, 2006; Masters and So, 2008). The value of 2P microscopy is that the behavior of individual cells can be studied in the context of their native 3-D environments within tissues including skin (Matheu *et al.*, 2008a; Peters *et al.*, 2008; Zinselmeyer *et al.*, 2008), spinal cord (Kawakami *et al.*, 2005), gut (Chieppa *et al.*, 2006), bone marrow (Cavanagh *et al.*, 2005; Celso *et al.*, 2008), and lymphoid organs (Aoshi *et al.*, 2008; Bousso and

Robey, 2004; Lindquist *et al.*, 2004; Mempel *et al.*, 2004a; Miller *et al.*, 2002, 2004a; Shakhar *et al.*, 2005; Witt *et al.*, 2005). Recently, 2P microscopy has been applied to study the dynamic interplay of host-pathogen interactions *in vivo* during viral, protozoan, and bacterial infection (Chieppa *et al.*, 2006; Egen *et al.*, 2008; Peters *et al.*, 2008). As the technology advances and new transgenic reporter mice and fluorescent probes become available, 2P microscopy will allow the immune response to be assessed at a functional level by providing readouts for intracellular signaling (Bhakta and Lewis, 2005; Bhakta *et al.*, 2005), gene expression, cell proliferation (Miller *et al.*, 2002), chemotaxis (Beuneu *et al.*, 2006; Castellino *et al.*, 2006; Hugues *et al.*, 2006; Okada *et al.*, 2005), and CTL killing (Boissonnas *et al.*, 2007; Mempel *et al.*, 2006).

2P excitation occurs when two longer-wavelength lower-energy photons (together having the equivalent energy of a single higher-energy photon) are absorbed as a single quantum of energy by a fluorophore, thereby promoting an electron to an excited state. From this point on, the process of fluorescence emission is identical to single photon excitation. The electron releases some of its energy through nonradiative processes and eventually (in the range of nanoseconds, www.olympusfluoview.com/) returns to its ground state, emitting the remaining energy as a lower energy photon. For 2P excitation to take place, the two photons need to be absorbed nearly instantaneously (within attoseconds). The high photon densities required for this low probability event to occur can be achieved by use of a microscope objective to focus a femtosecond pulsed Ti: Sapphire laser beam into a diffraction-limited spot (<1 μm) in the specimen. Because excitation effectively occurs only at the point of focus, the emitted fluorescence is localized in 3-D space. This allows the specimen to be optically sectioned by laterally scanning the laser spot in x and y dimensions and moving the laser focus sequentially in the z axis with an automated z-focus motor. The fluorescence emission is collected by photomultiplier tubes (PMT) at each point in the scan to build a digital image pixel by pixel. Z-stacks can be acquired repeatedly from the sample to generate 3-D time-lapse data. Once the images are collected, they are rendered in 3-D and cell analyzed quantitatively for velocity, colocalization, shape, volume, number, intensity, and color. Although 2P microscopy is expensive and the analysis time consuming, the technique provides single-cell spatiotemporal information that other imaging techniques cannot. In particular, 2P microscopy involves significantly less sample photodamage than confocal microscopy (this substantially improves cell viability) and, because of the reduced scattering of the infrared excitation light, images can be acquired several hundred microns deep in native tissues (compared with <80 μm with confocal microscopy) making it an extremely powerful technology for *in vivo* imaging (Masters and So, 2008).

2. 2P Microscope Systems

2.1. Scan heads and femtosecond lasers

In the past several years, 2P microscopy systems designed for biologic research have become commercially available. The recent trend is toward commercial laser-scanning microscope systems that are dedicated for 2P microscopy (i.e., without confocal detection capability and the added expense of visible lasers). The advantages of these commercial systems are that they are installed for the researcher, and service and maintenance is provided by the vendor. Moreover, these systems are designed to support a number of different imaging applications and often come with extensive user-friendly acquisition software and, in some cases, basic analysis software.

On the other hand, several researchers have chosen to build their own systems (Leybaert *et al.*, 2005; Nguyen *et al.*, 2001; Okada *et al.*, 2005; Tang *et al.*, 2006). Many technical details regarding the construction of these systems are posted on these researchers' web sites (URLs: http://parkerlab.bio.uci.edu/microscopy_construction.htm; http://users.umassmed.edu/michael.sanderson/mjslab/confocal_microscopy_main.htm; http://pathology.ucsf.edu//krummel/2PhotonHome.html). These sites are an invaluable resource for those interested in building their own systems. The advantage of a custom-built system is that it can be tailored to specific applications, such as intravital imaging, and optimized for sensitivity and speed. Moreover, once an investigator builds a system, they are in a position to further modify the equipment for new applications or quickly repair the system as needed without having to rely on the microscope vendor for service.

The 2P microscope built in our laboratory (Fig. 16.1) is based on Ian Parker's prototype instrument at UC Irvine (Nguyen *et al.*, 2001) but incorporates several further design improvements. First, the system is capable of capturing full-frame images at video-rate (30 f/sec) for up to four fluorescent detection channels simultaneously; whereas, commercial 2PE systems typically have two non-descanned detection channels and are limited to ~2 f/sec for the same scanned area and resolution. Recently, several commercial systems have introduced videorate scan heads as an option. These systems, using resonance (Leica) and accousto-optic device (AOD) scanning (Prairie), can also reach 30 f/sec. Rapid scanning is especially useful for quickly exploring the tissue for a region of interest and when analyzing highly dynamic phenomena such as leukocyte recruitment from the circulation.

A second novel feature of our system is that it is equipped with two tunable Ti: Sapphire lasers (Chameleon XR Ti: sapphire laser, Coherent) (Fig. 16.1A), which allows fluorescent probes with different optimal excitation wavelengths to be used simultaneously (e.g., YFP and CMAC),

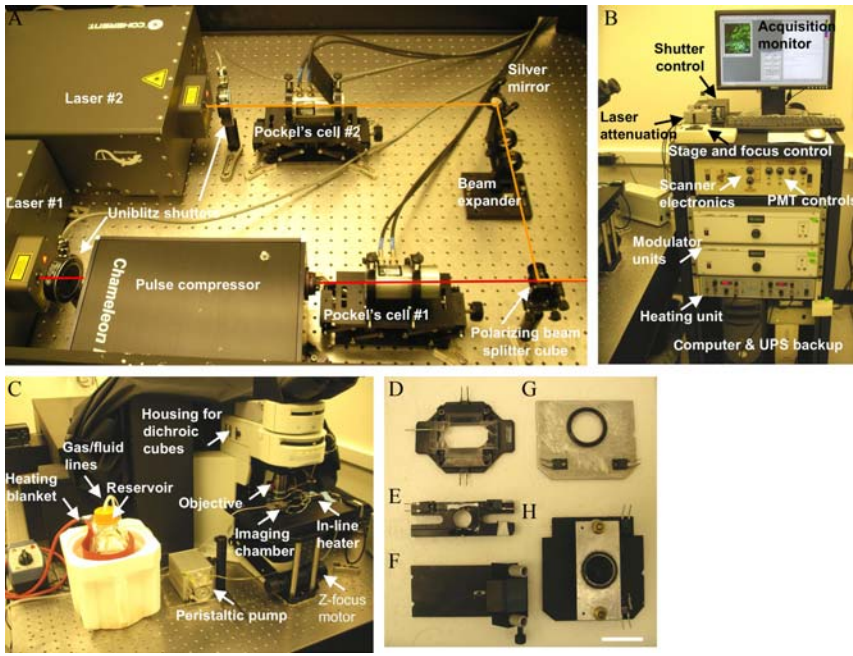

Figure 16.1 Dual-beam two-photon microscope system and imaging chambers. (A) optical layout of the system, showing the laser paths (red and orange) and crucial optical components. (B) Equipment rack containing acquisition computer, heating unit, modulator (Pockels cells) power supplies, scanner control electronics and PMT gain controls, joy stick for controlling the stage movement and focus, a potentiometer box to manually set laser attenuation, a shutter controller, and the acquisition monitor for viewing the specimen in real time. (C) Microscope stand and fluidics. Various imaging chambers for (D) explant tissue imaging (Harvard Apparatus), (E) ear imaging, (F) bone marrow imaging in the skull (with gas anesthesia connectors) (Harvard Apparatus), (G) footpad imaging, (H) intravital imaging of internal organs. Scale bar = 3cm.

which excite optimally at 915 nm and 780 nm, respectively. This makes it possible to discriminate complex mixtures of cells that cannot be separately identified by other 2P microscopes (Wokosin *et al.*, 2004) and to run internal controls (e.g., polyclonal T cells for antigen presentation experiments). Moreover, by alternating the laser lines with Pockels cells (Fig. 16.1A) as described in the section following, two probes with similar emission spectra, but different excitation optima, such as CMAC and CFP can be used together. This greatly expands the number of reporters that can be used in a single experiment. For example, in Fig. 16.2, a laser tuned to 900 nm was used to excite CFP, GFP, and YFP and a second laser tuned to 800 nm to excite CMAC and CMTMR. In this case the 900-nm and 800-nm images were acquired during alternate z-stacks (every 30 sec). This

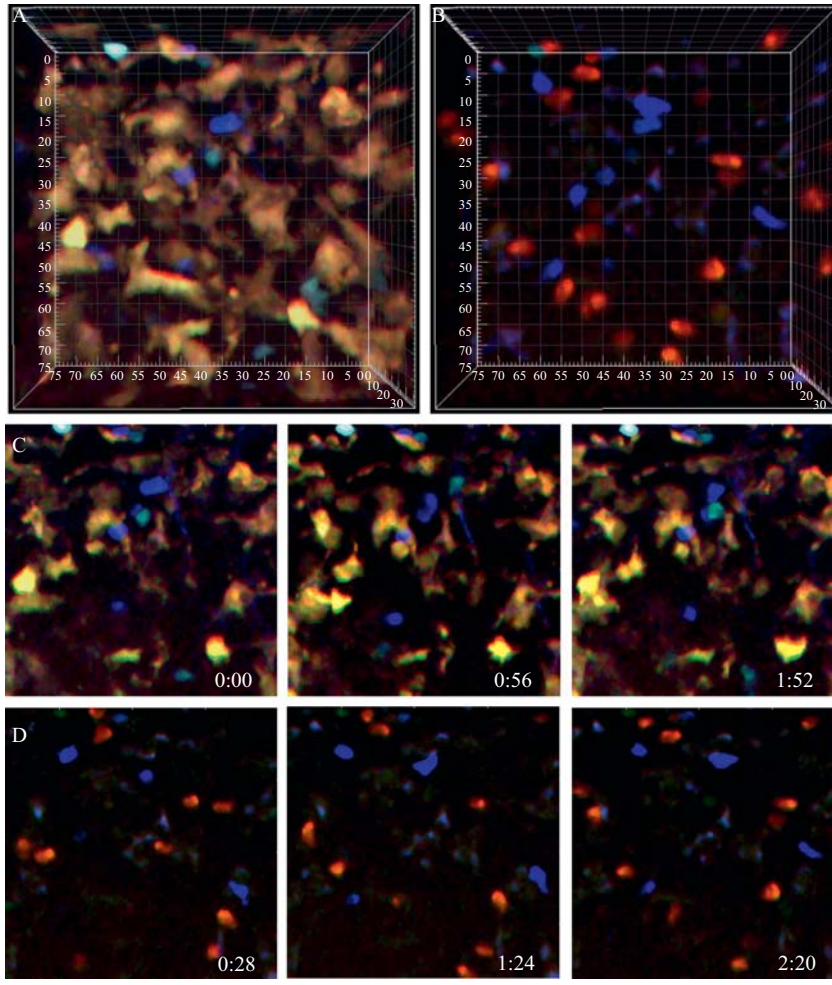

Figure 16.2 Imaging fluorescent proteins and fluorescent dyes with fast laser switching. Four different groups of $CD4^+$ T cells (2×10^6 each) were adoptively transferred into a CD11c-YFP transgenic mouse (Lindquist *et al.*, 2004). CFP- and GFP-expressing T cells were isolated from transgenic mice expressing these fluorescent proteins under the control of the actin-promotor (The Jackson Laboratory). Two other groups of T cells had been stained with CMTMR and CMAC. (A) 3-D view of lymph node excited at 920 nm (Laser #1), showing YFP^+ dendritic cells (yellow); GFP-expressing T cells (cyan), and CFP-expressing T cells (blue). (B) The same field of view excited at 790 nm (Laser #2), showing CMTMR-labeled T cells (red) and CMAC-labeled T cells (blue). (C and D) Three time-lapse images where the laser excitation was alternated between (C) 920 nm and (D) 790 nm. Times are indicated in min:sec.

is sufficient for many applications, but the laser lines could also be switched during each z-step, enabling imaging of four fluorescent proteins and four fluorescent dyes with only a 33 to 500 msec time difference.

2.2. Acquisition software

We developed custom software (ImageWarp, A&B software) in collaboration with A&B software (Boris Nalibotski), to perform on-the-fly image correction (for the Raven camera board, Bitflow) and to control hardware components, such as the z-focus motor and laser shutters (Fig. 16.1B). Multi-dimensional data files (intensity, color, time, and three spatial dimensions) are streamed to a lab server (X-Serve with 3.75 Tb capacity RAID5 array, Apple inc.) after the acquisition. Others have used Video Savant (IO Industries) or Slidebook (Intelligent Imaging Innovations Inc.) as their acquisition and hardware control software. The preferred formats for multi-dimensional data files are either tiff stack (compatible with a wide range of software platforms) or Metamorph stk files, which are archived and accessed efficiently. Importantly, formats should be recognized by commercially available software for image rendering and analysis such as Volocity (Improvision) and Imaris (Bitplane). Although automated tracking software works for many applications, manual tracking is often necessary in experiments in which cell densities are high or in situations in which intensity thresholding is problematic. In any case, we found it useful to use manual tracking software such as Picviewer (compatible with tiff, stk, and pic files, John Dempster) to validate the results obtained with automated tracking software, because automated tracking can be prone to errors.

2.3. Signal detection and optical filters

Our system uses four multi-alkali PMTs (Electron tubes) mounted in the epifluorescence module, as close as possible to the back aperture of the objective (XLUMPlanFI 20x/0.95NA waterdipping, Olympus) (Fig. 16.1A). The box contains a rail to hold up to three Olympus filter cubes in series. For most applications, we use high-efficiency dichroic filters (Semrock) for separating the fluorescence emission, without added bandpass filters. This configuration maximizes detection efficiency at the expense of clean channel separation. In most situations, moderate signal crosstalk does not impair cell tracking or performing morphometric analysis. However, signal bleedthrough can cause problems for automated tracking software. If automated tracking is to be performed later, it may be necessary to install bandpass filters to "clean up" the channels, but this comes with a cost. Because bandpass filters reduce the signal intensity, more laser power must be used to achieve comparable signal, which may adversely impact cell viability in the specimen.

Our advice is to purchase a filter cube with each dichroic mirror and clearly label it to facilitate swapping the filters in and out of the system and to prevent them from getting lost, damaged, or mixed up. The dichroic

mirrors (for separating fluorescence emission) we have found most useful for separating commonly used fluorescent probes in our laboratory are:

458 nm; 2nd harmonic generation signals
480 to 490 nm; CMAC and CFP
505 nm; GFP (505 nm divides GFP into blue and green channel; therefore, cells are cyan and can be easily distinguished from YFP)
525 nm; GFP
540 nm; YFP
560 nm; Rhodamine-dextran, CMTMR, RFP
590-nm; CMTPX, 605-nm FluoSpheres, or 655-nm quantum dots.

It is important to check the dichroic filter transmission spectra below 400 nm. This is an issue with 2P microscopy because second and third harmonic generation signals will bleedthrough into the longer wavelength channels. To prevent shorter wavelength light from contaminating other channels, make sure the first dichroic filter, in the series (i.e., the blue filter) has good blocking characteristics into the 300-nm range.

Emitted fluorescence collected through the objective lens is reflected into the detector head by a dichroic mirror that transmits the IR wavelengths (>680 nm) of the excitation laser beam. The cube holding this dichroic also includes a barrier filter to block laser light reaching the detectors. Selection of this filter is crucial, because the laser beam is many orders of magnitude brighter than the fluorescence signals, and dichroics and filters specially designed for multiphoton applications are available from several suppliers. We have also found it necessary to place a long-pass (>680 nm) filter in the laser excitation path to block low levels of visible wavelengths emitted by the Chameleon laser.

2.4. Laser attenuation and fast shuttering

The laser beam from each Chameleon laser is routed through an electro-optical modulator to enable precise and rapid control of the power at the sample plane. The modulators (M350-50-02-BK, ConOptics) can reduce the laser power by the full extinction ratio (~400:1) over the tuning range of the lasers. The M350-50 modulator uses 50 mm of potassium dideuterium phosphate (KD*P) birefringence crystal (two crystals of 25 mm), and yields an effective interaction region for the Pockels effect of 3.1-mm diameter. The modulator crystal cavity is filled with index-matched fluid (FC-43, n~1.291) to provide a device with low insertion loss and very high damage thresholds. The broadband antireflection coating wavelength range is 700 nm to 1200 nm (−02) and has been verified to have 5% insertion loss over this entire wavelength range. The KD*P series crystals (M350) have intrinsic piezoelectric resonances near 64 kHz, which can cause sustained ringing with rapid voltage changes and can also introduce spatial problems

with the exiting laser beam profile. A special resonance clamped option (−BK) has been introduced to move these resonances past 200 KHz to better match to the frequency range possible with KD*P modulators and the M302 drivers. The input drive voltage (0 to 2V) is amplified by ~375 times by the modulator driver (M320RM, ConOptics) before being applied to the crystals. A full change in transmission intensity requires ~5 μsec with this driver and modulator combination. The modulators were installed with the polarizer parallel to the plane of polarization of the laser, which is parallel with the top of the antivibration table. Thus, 0V drive voltage results in maximum power transmission.

2.5. Sample power control

A custom-written Delphi program was created (*PowerCal*, John Dempster) to calibrate and control the electro-optical modulators from a personal computer with a digital-to-analog voltage card (PCI-6014, National Instruments) by means of drive voltage output signals. The parallel polarizer modulator configuration requires a $\cos^2$ equation to relate the drive voltage to the actual transmission. Longer laser wavelengths require more drive voltage to achieve full extinction, so the drive voltage is normalized by a wavelength dependent value, V_π, for a full $\lambda/2$ shift in polarization. The *PowerCal* program also features a rapid end-of-frame triggering option that can be controlled by an ImageWarp script (Jonathan Cannon) to alternate the two modulators between the imaging sample power and minimum sample power (full modulator extinction). With this ratiometric mode, we were able to acquire stable, alternating excitation wavelength imaging at 30 frames per second. The Chameleon laser output power is ~1.5 W at 780 nm (and less at other wavelengths), which poses no detectable thermal heating drifting effects of the M350 modulator transmission. Higher laser powers (>2 W into 1 mm^2) have been shown to induce an exponentially varying signal with time. A separate potentiometer box was created to derive the modulator drive voltages; this permitted manual control of the sample power for each laser. This manual/remote feature is often used during initial image acquisition with the fast scanning system.

2.6. Pulse compression

As the TI: sapphire laser passes through the optical components of the system, the laser pulse becomes broadened (positive dispersion), because the longer wavelengths of light travel faster through these materials. Pulse dispersion can substantially lower the peak power of the laser at the sample and, therefore, decrease the efficiency of 2P excitation. To correct for dispersion in the system, precompensation is performed with a set of prisms (Fork, 1986) to introduce negative dispersion (slowing down the longer

wavelengths of light) and restore the pulse width at the sample. Our system uses a prism-based pulse compression unit (FemtoControl, Coherent), which in our hands has yielded increased excitation efficiency and tissue imaging depth (~30 to 50% deeper).

3. Fluorescent Reporters

Although 2P microscopy can be achieved by use of intrinsic signals (autofluorescence, second-harmonic generation), many applications require that specific cell populations be fluorescently labeled. This is most often accomplished by staining cells with vital fluorescent dyes or by expressing genetically encoded fluorescent protein in a cell lineage specific manner.

3.1. Fluorescent dyes

One approach that has worked well with leukocytes is to isolate the cell type of interest by magnetic bead separation or density gradient centrifugation and label the cells with fluorescent dyes (Matheu and Cahalan, 2007). CellTracker probes CMAC, CFSE, CMTMR, CMTPX (Invitrogen) are commonly used for this purpose, as well as other dyes such as SNARF, which works well in combination with CFSE (Germain *et al.*, 2005). A typical staining protocol for leukocytes (T cells, B cells, bone marrow neutrophils, and freshly isolated splenic DCs) is described in the following and summarized in Table 16.1.

The dye concentrations in this table have been optimized to balance the fluorescence intensity of cotransferred leukocyte populations during subsequent imaging.

3.1.1. Dye-labeling protocol for leukocytes

Stock solutions are made by dissolving lyophilized dyes in DMSO to achieve the following concentrations: 20 m*M* CMAC, 10 m*M* CFSE, CMTMR, and CMTPX. For CFSE and CMTPX, which come in predispensed 50-μg vials, add 7.3 μl DMSO to the tube and vortex or flicking the tube vigorously with your finger to redissolve the material. Dyes can be aliquoted and stored at -20 °C for several months. Freezing and thawing the stock solutions multiple times should be avoided.

Cell staining works well in CO_2-independent medium (Gibco). When staining with CMTPX, we suggest adding 1% BSA to the medium to improve cell recovery. The cell density during staining should be approximately 10×10^6 cells/ml (for less than 10×10^6 cells use 1 ml). Dilute the stocks as in Table 16.1, into a 15-ml Falcon tube. For example, to stain 40 million cells with CMAC, 4 ml of 50 μM staining solution will be needed.

Table 16.1 Summary of a leukocyte staining protocol optimized for two-photon imaging

Dye	Stock solution 7.3 μl DMSO to 50-μg vial	Final concentration	Medium	Incubation @ 37 °C
CMAC	20 m*M*	2.5 μl Stock into 1 ml medium = 50 μM	CO_2 independent	40 min
CFSE	10 m*M*	0.5 μl Stock into 1 ml medium = 5 μM	CO_2 independent	30-40 min
CMTMR	10 m*M*	1 μl Stock into 1 ml medium = 10 μM	CO_2 Independent	40 min
CMTPX	10 m*M*	1.5 μl Stock into 1 ml medium = 15 μM	CO_2 independent + 1% BSA	40 min

Pellet the cells in a 15-ml Falcon tube by centrifugation at 300*g* (neutrophils require ~800*g*) for 6 to 10 min. Carefully remove the supernatant, and resuspend the cell pellet in 1 ml of CO_2 independent medium with vortexing. In a separate tube, add 10 μl of 20 m*M* CMAC stock solution to 3 ml of medium and mix thoroughly. Add the 3 ml of staining solution to the 1 ml of resuspended cells and mix well by pipetting up and down several times. This approach ensures that the cells are stained homogeneously.

Incubate the tube at 37 °C for 40 min, mixing the 15-ml Falcon tube twice during the incubation period. After the incubation, fill the tube with cold medium and centrifuge (6 to 10 min at 300*g*). Remove the supernatant and wash once more if desired. Resuspend the pellet in 200 to 250 μl of PBS for adoptive transfer. Stained cells should be not stored for more than a few hours at 4 °C, whereas unstained cells can be stored overnight at 4 °C and labeled the next day with ~20 to 25% loss in cell number.

3.2. Genetically encoded fluorescent proteins

Alternately, experiments can use transgenic mice that express fluorescent proteins in a lineage-specific fashion. In our hands, several transgenic models have excellent 2P imaging characteristics; CD11c-eYFP (for dendritic cells

[Lindquist *et al.*, 2004], CX3CR1 for monocytes and dendritic cells [Geissmann *et al.*, 2003], LysM-eGFP for monocytes and neutrophils [Faust *et al.*, 2000]). In these models, cells are brightly labeled, and the expression is reasonably specific with minimal background expression. In addition, transgenic mice expressing global CFP, GFP, YFP (The Jackson Laboratory), and RFP (Vintersten *et al.*, 2004) driven by the chicken β-actin promoter is useful in cases in which the cells of interest can be isolated and adoptively transferred into suitable recipient strains. In the transgenic models mentioned previously, the fluorescent protein expression level is high, and cells can be detected easily with 2P microscopy. However, this is more often the exception rather than the rule. As a general guideline, if the fluorescence intensity of the cell of interest is $\sim$2 units over background by flow cytometry, then the cells are likely bright enough to be imaged by 2P microscopy.

3.3. Autofluorescence and second harmonic generation signals

Also, tissues and cells can emit intrinsic signals that are useful as tissue landmarks. These include the second harmonic generation signal produced as the 2P laser interacts with non-centrosymmetric materials such as collagen in the skin and connective tissues (Gauderon *et al.*, 2001; Zoumi *et al.*, 2002). For excitation at 900 nm, a second harmonic generation signal at 450 nm will be produced (half the wavelength of the incident light). Some tissues, for example skeletal muscle (Rothstein *et al.*, 2005) and pancreatic islets (Rocheleau and Piston, 2003), have strong autofluorescence because of NAD(P)H and flavoproteins. In some cases, autofluorescence is bright enough to visualize individual cells without labeling, such as with certain macrophages.

4. Imaging Preparations

2P imaging preparations generally take three main forms: (1) explanted tissues and intact organs placed under the flow of suitable medium; (2) invasive intravital imaging and; (3) noninvasive imaging of accessible surfaces, such as the skin or cornea.

4.1. Explant imaging

Despite the caveats associated with explant preparations, they are undoubtedly more physiologic than most *in vitro* cell systems and have the additional advantages of being easy to work with (compared with intravital imaging preparations), yielding robust and reproducible results and allowing tissues to be studied that cannot be accessed otherwise. Moreover, they minimize

animal welfare issues that might arise with live animal imaging studies. In many cases, explant imaging yields results indistinguishable from intravital imaging (Mempel *et al.*, 2004a; Miller *et al.*, 2002; Shakhar *et al.*, 2005). Because explant studies can be performed more quickly and easily, it is useful to use this approach initially and perform a limited number of intravital experiments to validate the results.

The methods described in the following sections were developed for imaging lymphoid tissues, and for simplicity we will focus on those tissues. However, with only slight modifications explant imaging can be successfully used to examine a diverse range of nonlymphoid tissues including the brain, kidney, lung, liver, stomach, gut, and bone. Although explanted preparations are often a significant improvement over existing *in vitro* models, it is possible that the loss of blood flow and innervation might alter host cell behavior. This was an initial criticism of explanted lymph node imaging studies (von Andrian, 2002), but cell behaviors were shown subsequently to be remarkably similar in explant and intravital preparations (Mempel *et al.*, 2004a; Miller *et al.*, 2002, 2003; Shakhar *et al.*, 2005).

4.1.1. Explant imaging protocol

See Matheu *et al.* (2007) for a video illustrating these procedures: The animal is euthanized and the tissue harvested and placed in a small Petri dish containing medium. Our laboratory uses CO_2- independent medium (Gibco); most tissues remain viable for several hours stored at room temperature in this medium. Placing tissues on ice might be beneficial in some cases, but in our experience room temperature works best with lymphoid tissues.

The tissue of interests is then glued to an unbreakable plastic coverslip (Fisher). Cut the coverslip to the appropriate size (i.e., big enough to hold the tissue, but small enough to fit in the flow chamber) and apply a thin layer of veterinary grade superglue (VetBond, 3M) with the small piece of paper that separates the coverslips in the box. Leave one corner uncoated for manipulating the coverslip later. To prevent rolling the sample in the glue, place the tissue on the coverslip in one smooth movement with a small pair of curved forceps. It is helpful to hold the cover slip firmly to the bench with a second pair of curved forceps placed on the unglued corner. The tissue must be placed on the coverslip within ~1 min of spreading the glue or the tissue might fail to adhere properly. To prevent the excess glue on the coverslip from "shrink wrapping" the tissue when you place it back in the Petri dish, invert the tissue and dip it into the medium tissue side down to cure the remaining glue. Once the glue is cured, the coverslip can be placed tissue side up in the petri dish and stored at RT until imaging.

In some tissues where imaging depth is limited, such as the spleen, it may be necessary to section the tissue to expose the regions of interest (Aoshi *et al.*, 2008). Secure the spleen to a plastic coverslip with a thin film of VetBond as described previously. Section the spleen longitudinally with a

Vibratome (Pelco) set to speed 3 and displacement 5, remove ~500 μm of the overlying red pulp and expose the marginal zone and the white pulp. The angle of the blade is critical; try experimenting with different angles until sections are cut cleanly and consistently. There is concern that sectioning the spleen will damage the tissue and alter cell behavior; therefore, image white pulp regions that seem to be intact on the basis of the presence of a ''cap'' of undamaged marginal zone macrophages.

The flow chamber should be set up 15 to 30 min ahead of time to allow the flow chamber to equilibrate at 37 °C before imaging is started. It is important to submerge the objective into the medium to stabilize the bath temperature and prevent bubbles from forming later (i.e., when a room temperature objective is placed in 37 °C medium). The ceramic surface of the objective is a good insulator and heating the objective is not necessary in most cases. We use a peristaltic pump (Watson-Marlow) to deliver media from a reservoir (500-ml round glass bottle) to the inline heater, which is attached to the flow chamber (Warner) (Fig. 16.1C). Microwave the bottle of medium first for several minutes to warm it and then maintain the temperature at 37 to 45 °C with a heating blanket (place the bottle and heating blanket in a Styrofoam bucket for insulation) (Fig. 16.1C).

For tissue culture media that is designed for use in a 5% CO_2 incubator, we bubble carbogen gas (5% CO_2, 95% O_2) through an aquarium air stone placed in the reservoir (Fig. 16.1C). This serves to oxygenate the media and stabilize the pH, (i.e., dissolved CO_2 is important for regulating pH in tissue culture media). There is some controversy about how much oxygen is required to maintain physiologic motility of cells, but protocols range from 20 to 95% (Germain *et al.*, 2005; Huang *et al.*, 2007; Miller *et al.*, 2002). Carbogen gas has worked well in our hands, and we suspect that the amount of O_2 dissolved in the medium is relatively low by the time it reaches the chamber. However, this protocol might not work well for every tissue, and the reader is advised to consult the scientific literature for additional information.

We have used a variety of media to maintain the tissue during imaging. Usually what works well for tissue or organ culture will work well for explant imaging too. One notable exception is that fetal calf serum (FCS) should be left out of the media, because bubbling carbogen will cause it to froth (and create a sticky mess on the optical bench). For explant imaging, FCS is most likely unnecessary, because cells are within their native tissue environments. For lymphoid tissues RPMI (Miller *et al.*, 2002, 2004b) or DMEM works well. For spleen explant imaging where the spleen has been sectioned with a Vibratome, we found that high-glucose DMEM minimizes tissue swelling and improves imaging results (Aoshi *et al.*, 2008). Although we use DMEM without phenol red, it is unlikely that the indicator dye interferes substantially with imaging, because RPMI with phenol red works well in our hands.

If a tissue swells or shrinks, it likely indicates that either the temperature is fluctuating or that the medium is not isotonic with the tissue. First, verify that flow of medium is constant and the heating unit is working properly.

If this does not solve the problem, try adjusting the osmolarity of the medium (e.g., if the medium appears hypotonic and the tissue is swelling, try adding extra glucose to make the medium isotonic).

In our experience, explanted lymphoid tissues remain viable for 4 or more hours, but each tissue will be different, and some tissues, such as the pancreas, are difficult to preserve. As a general rule, imaging should be limited to several hours to ensure that the images are representative of *in vivo* behaviors. Any wholesale decline in cell motility or loss of cell morphology could indicate that the preparation is no longer viable.

4.2. Intravital imaging

Various intravital chambers (Fig. 16.1E-H) have been developed to stabilize lymph nodes for imaging and maintain blood flow and lymphatic drainage (Lammermann *et al.*, 2008; Lindquist *et al.*, 2004; Mempel *et al.*, 2004a; Miller *et al.*, 2003). These preparations maintain tissue viability for several hours based on the preservation of cell motility (a rapid decline in leukocyte motility is an indication that the tissue is no longer viable).

4.2.1. Intravital imaging protocol

The mouse is anesthetized with isoflurane delivered in a stream of O_2. Anesthesia is induced at 4% isoflurane, and once the animal becomes unresponsive (assessed by toe pinch), the isoflurane can be lowered to 1.5 to 2% to maintain anesthesia. Isoflurane provides stable and convenient anesthesia for most intravital imaging preparations. In particular, B6 mice respond in a highly predictable fashion and can be anesthetized with isoflurane for several hours without serious side effects. However, other strains of mice, for example BALB/c mice, can respond less predictably. The respiration rate of the mouse should be monitored closely to fine-tune the plane of anesthesia. If isoflurane does not work for a given mouse strain or preparation, injectable anesthetics might be more suitable, such as Avertin (1.2% Avertin is given i.p. at an initial dose of 0.02 ml/g, with supplemental doses of one half the initial bolus given at a frequency of ~45 to 90 min) or a combination of ketamine, xylazine, and acepromazine (s.c. injection of 100 mg ketamine, 15 mg xylazine, 2.5 mg acepromazine per kg and anesthesia maintained with hourly injections of half the induction dose). To prevent the mouse from becoming dehydrated, administer PBS or saline (100 μl, s.c.) every 1 to 2 h as needed.

To image the inguinal lymph node, make a midline incision in the lower portion of the abdomen with round-tipped surgical scissors. Take care not to cut through the peritoneal membrane. Gently pull away a flap of skin containing the inguinal lymph node and glue (Vetbond, 3M) a rubber O-ring (17-mm outside diameter, centered over the lymph node) on the inner side of the skin flap. Place the mouse in the imaging apparatus on top of the warming plate (35 to 36 °C, to help regulate the mouse's body temperature). Insert the O-ring into a flanged Plexiglas support and

secure the tissue between the support and the heating platform. Be careful not to compress the tissue and cut off the blood flow to the lymph node. Seal the O-ring with petroleum jelly to prevent the objective immersion medium (PBS or saline) from leaking out. Maintain the imaging chamber temperature at 35 to 36 °C with a thermistor placed in the liquid.

If the lymph node is covered by a layer of fat (this is often the case for inguinal lymph nodes), the fat will severely degrade, the quality and depth of imaging. Therefore, we recommend removing the fat pad with fine-tipped Dumont forceps. Removing the fat should be performed carefully under a dissecting microscope to avoid breaking blood vessels or damaging the lymph node. Alternately, the lymph node can be imaged through naturally occurring ''windows'' in the fat pads that are frequently seen in young mice (~4 weeks old).

To image blood vessels and assess blood flow in the lymph node, we inject i.v. or retro-orbitally 10 to 20 mg/ml tetramethylrhodamine dextran (2000 kDa, Invitrogen) or 20 μl of 655-nm nontargeted quantum dots (Invitrogen).

In many cases, imaging the popliteal, inguinal or cervical lymph node is possible. The popliteal and inguinal imaging preparations have been well described (Memple *et al.*, 2004b; Miller *et al.*, 2003; Shakhar *et al.*, 2005). Imaging cervical lymph nodes is advantageous, because they do not have a tightly associated fat pad and the lymphatic drainage is highly predictable (i.e., injecting the ear or nape of the neck drains to the cervical lymph nodes reproducibly). For imaging the cervical lymph nodes, our approach is essentially the same as for the inguinal lymph node preparation, except we use our intravital imaging chamber (Fig. 16.1H) (Miller *et al.*, 2003).

Make a small incision longitudinally along the throat. A small skin flap containing the cervical lymph nodes can be mobilized and inverted with the index finger and thumb. If necessary, any overlying tissue can be gently moved to the side with a fingertip or forceps while maintaining pressure from the index finger from the outer side of the skin flap.

Apply VetBond to the underside of the glass coverslip of the intravital chamber (Fig. 16.1H), leaving a small ''glueless'' window in the center.

Lower the coverglass over the tissue guiding the lymph node into the glueless window. Gently press the tissue into the glass until firm contact is made. The surrounding tissue will become glued to the coverglass and support the lymph node against the window. If a small amount of glue comes in contact with the lymph node, the preparation will still work; however, it is best to avoid contact as much as possible.

4.3. Imaging peripheral tissues

In some cases it is possible to image in a purely noninvasive fashion such as in the ear (Matheu *et al.*, 2008a,b; Peters *et al.*, 2008), footpad (Zinselmeyer *et al.*, 2008), or eye (Yeh *et al.*, 2002). This approach is particularly useful for examining host effector responses to infection in peripheral tissues.

4.3.1. Noninvasive imaging protocol

The animal subject is anesthetized with isoflurane delivered in a stream of O_2. Anesthesia is induced at 4% isoflurane, and once the animal becomes unresponsive (assessed by toe pinch), then the isoflurane is lowered to 1.5 to 2% to maintain anesthesia. During imaging experiments with live mice, the mice are deeply anesthetized with isoflurane for restraint and to minimize stress on the animal subject. The depth of anesthesia should be assessed throughout the procedure by checking for the absence of a toe pinch reflex and by monitoring the respiration rate.

To secure the paw or ear to the imaging apparatus (Fig. 16.1E,G), we apply a thin film of VetBond (3M) tissue adhesive to the glass surface of the chamber and hold the tissue in place by applying gentle pressure for 10 to 15 sec or until it is securely attached. In some cases, it might be necessary to use a thin film of higher viscosity and faster drying adhesive (superglue gel) to hold the tissue.

For footpad imaging, the chamber (Fig. 16.1G) is filled with PBS. For ear imaging a drop of PBS is placed between the ear and the objective and held in place by surface tension alone. This approach works particularly well for the inside surface of the ear, because the ear itself creates a natural fluid chamber.

The mouse's core body temperature is maintained by placing it on a warming pad (Braintree Scientific) set to 37 °C and supplemental fluids (saline) are administered i.p. or by retro-orbital injection as needed.

We inject (i.v. or retro-orbital) or 1 mg/ml dextran, tetramethylrhodamine, 2,000,000 MW (Invitrogen), or 20 μl of quantum dots to label blood vessels during imaging.

In many cases, peripheral tissues can be imaged for up to 4 h without compromising the normal physiology of the tissue. Typically the mouse is euthanized while under anesthesia. However, longitudinal imaging studies are also possible with this approach, because it is noninvasive and does not harm the animal. If the mouse is to be revived for longitudinal studies, we recommend imaging for shorter periods of time (~2 h) to minimize the risk of dehydration or anesthesia overdose and imaging no more than 5 time points in 10 days.

5. Image Acquisition

Carefully choosing the acquisition settings is crucial to ensure that the experiment can be successfully analyzed (Fig. 16.3). If the signal is too low, the cell density too high, or the time resolution inappropriate for the phenomena one wishes to study, then the analysis is doomed from the start. Also, the local tissue environment can have a significant impact on cell motility and function; therefore, if possible, include an internal control population of cells to compare, side-by-side, with the behavior of your cell

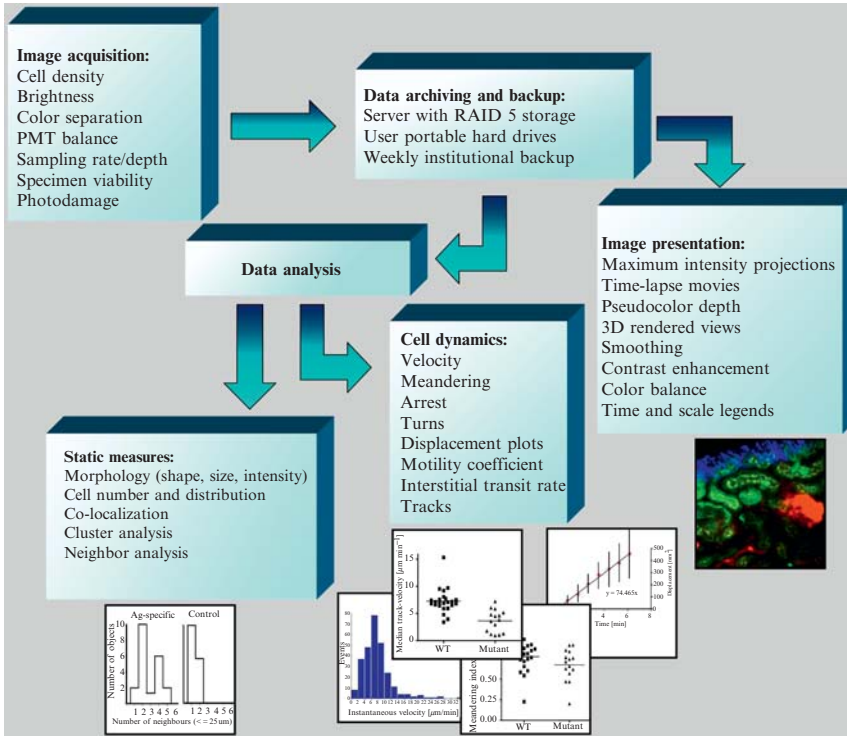

Figure 16.3 **Flowchart illustrating the various considerations and procedural steps from image acquisition to analysis and the presentation of results.**

of interest. Examples of internal controls include cotransferring polyclonal T cells along with antigen-specific T cells to examine antigen recognition or comparing gene-deficient and wild-type cells side by side.

5.1. Laser power and PMT gain

Laser intensity and PMT gain must be set carefully to minimize photodamage to the tissue and to avoid oversaturation of the acquired images. To preserve cell viability, set the laser power (exposure dose) as low as possible and adjust the PMT gain as high as possible to optimize the signal-to-noise ratio. The cells of interest should be 3 to 10-fold greater in intensity compared to the highest background level. Be careful not to saturate the signal; if pixels flare or are reading close to the maximum gray level (256 on our 8-bit acquisition system), the laser power should be reduced. If the laser power and PMT gain are properly set, cells should remain motile and viable within a 1 to 2 h imaging window. A key factor is how much laser energy

the cells are exposed to during the experiment. For example, if images are taken every 30 sec with 15 frames averaged (0.5 sec per z-step) and 31 z-steps with ~25% relative laser power (Chameleon XR tuned to 900nm), leukocytes will remain motile for the entire 1 hr imaging record. When events need to be followed over a long period of time, one can sacrifice time resolution for duration. Therefore, to image for 2 h with equivalent photodamage to 1 h, take a time point every 1 min instead of every 30 sec. This is only a general rule of thumb, and viability will vary substantially depending on the laser wavelength, the dyes used, the tissue imaged, and the cells of interest. However, we do not mean to imply that laser power and exposure duration are perfectly linearly interrelated. In our experience, cell damage seems to increase as a steep function of laser power so that, for example, a doubling in exposure time has little effect, whereas a 30% increase in power may rapidly kill cells. Keep in mind that if the cells are slow-moving or sessile (dendritic cells for example), they will accumulate more photodamage than highly motile cells or cells flowing in the circulation that are exposed to the laser for a shorter amount of time.

When the experiment involves two or more colors, an attempt should be made to match the intensity of each channel. This can be accomplished by adjusting the dye conditions, adjusting the gain separately for each channel or by choosing a laser excitation wavelength to favor a dimmer fluorescent probe over a brighter one. For example, if CFSE is too bright when imaging with CMTMR, tune the 2P laser wavelength from 780 nm to 820 nm to balance the signals. The longer laser wavelength will excite CMTMR more efficiently and increase its brightness, while at the same time decrease CFSE excitation and fluorescence.

5.2. Cell density

If densities are too high, it becomes difficult to unambiguously track individual cells. Conversely, although it is easy to track sparsely distributed cells, the "*n*" numbers for statistical analysis become distressingly small. It is often helpful to use different concentrations of cells in experiments for quantitative analysis versus those aimed at producing movies for presentations and online publication.

5.3. Z-series acquisition and time resolution

The size of the observed volume and the number of z-planes has to be chosen carefully. The minimum distance between z-planes in the 3-D stack is set on the basis of the axial resolution of the 2P microscopy, which is typically 1.5 μm and on the thickness of the cells of interest (~4–10 μm for leukocytes). If you only want to track a cell's position, the z-step can be quite large, the criterion being that a cell cannot "disappear" between

successive planes. A larger number of z-steps will provide a larger imaging region and allow cells to be tracked for longer distances. However, the more z-planes acquired, the slower the acquisition time for the complete volume, the longer the time interval between time points and the lower the tracking precision. With a microscope scanning at video rate and 15 frames averaged for each full frame, typical volumes of $200 \times 250 \times 75$ μm (21 z-planes, 2.5 μm/step) can be acquired at intervals of 25 to 35 sec. Averaging 10 to 30 frames at each z-plane can substantially increase the contrast of the image, but the tradeoff is that the time resolution between frames is decreased, which can cause fast-moving cells to appear stretched or be blurred in the images.

6. Multidimensional Analysis

Once the data are in hand, the painstaking process begins of analyzing the data and generating plots, figures, and movies (Fig. 16.3). One good day of imaging can generate a week's worth of analysis.

6.1. Cell detection

The raw data produced by the laser-scanning microscope is a series of 3-D image stacks containing one or more fluorescence intensity channels, depending on how many different fluorophores were used in the experiment. To facilitate the analysis of cell movement and behavior, the location of cells within each 3-D image stack must be determined and the path of each cell tracked between successive time points.

Within a 3-D image, fluorescently labeled cells appear as objects consisting of contiguous blocks of bright against a relatively dark background. The high-contrast ratios and the fact that cells appear as single objects with little internal ultrastructure allow simple intensity threshold–based criteria to be used to detect objects. It is important to note that bright spherical objects tend to elongate in the z-dimension. This phenomenon was described in the early days of confocal microscopy (White *et al.*, 1987). Nevertheless, the magnitude and mechanism of elongation along the z-axis is controversial (Lee *et al.*, 2008). This elongation is especially pronounced with 2P microscopy, because the voxel resolution in the z-axis is typically 1.5 μm or more. This phenomenon must be taken into consideration when rendering the data in 3-D and can be minimized by use of the minimum laser power necessary and avoiding oversaturating the PMTs.

An intensity threshold is defined, which separates the brightly fluorescent cell from the dim background. An appropriate threshold level can be obtained by plotting an intensity profile through the midpoint of a typical cell and the surrounding background, setting the threshold midway

between the peak cell intensity and background intensity. In most cases in which a good contrast ratio is available, slight variation in the chosen intensity threshold has little impact on cell motility measurements. However, it is worth noting that cell volume measurements will be greatly affected by threshold setting, with lower thresholds including more within the object and hence increasing the apparent volume.

Once a threshold has been defined, the within each 3-D stack are classified into sets of objects, defined as contiguous groups of threshold-exceeding, within each plane and on adjacent planes within the stack. A volume-limit criterion is then usually applied so that objects below a predefined volume (e.g., single pixels and other small artifacts) are discarded. The 3-D location of a cell is typically defined as it centroid, computed as the mean location of the within the object. The volume of the object can be computed from the number of and the known dimensions of each.

6.2. Cell tracking

Tracking of cells requires the identification of the object corresponding to each particular cell within the 3-D image at successive time points. This can be done manually or automatically. Although the threshold-based detection of objects is straightforward with standard algorithms, the automatic tracking of objects is more problematic. Cells can be matched between time points by a variety of criteria: volume, shape, overlapping volume, distance of separation. However, cells change shape, orientation and apparent volume between time points move in and out of the imaged volume, merge, and separate. The automatic algorithms currently available cannot be relied on to unambiguously track individual cells under all conditions with 100% reliability. Consequently, careful scrutiny of the results of automatic tracking algorithms, with the ability to manually edit or delete putative tracks, is essential. Given the need for such inspection and validation, manual tracking of objects by the user can be just as effective and no more time consuming.

The two most widely used, commercially available, packages capable of the automatic detection and tracking of objects in 3-D are Imaris (Bitplane, Zurich, Switzerland) and Volocity (Improvision, Coventry, UK). We ourselves have also used an open source package PicViewer (J. Dempster, University of Strathclyde) capable of automatic object detection and manual object tracking.

6.3. Cell and tissue morphology

Although a primary application for 2P microscopy is to study single-cell motility, the 3-D nature of the technique provides several further useful measures. Simple observations such as the shape of cells (Miller *et al.*, 2002), the

number of cells, or the 3-D distribution of a cells in a tissue can be be highly informative. 2P microscopy can help visualize the 3-D arrangement of cells in native tissues and provide insight that is difficult to glean from fixed section imaging. Moreover, 2P microscopy can allow researchers to correlate differences in cell morphology and cell behavior between different tissue locations (Millington *et al.*, 2007).

6.4. Cluster and neighbor analysis

Under many conditions, groups of two or more cells are found clustered together, showing relatively little movement during the typical imaging period (30 to 60 min). It is difficult to investigate directly the time course of these long-lasting clusters; however, the number and size of individual motile cells and stable cell clusters found during a imaging period nevertheless provides an insight into cellular activity, with differences being readily demonstrable between different immunologic states (Zinselmeyer *et al.*, 2005) Cell clustering can be quantified in terms of the number of cells in contact with each other or within a certain radius of each other (Gelman *et al.*, 2009).

Contact clusters appear as single objects with volumes larger than expected for single cells. With an estimate of mean cell volume obtained from single motile cells, the number of cells in each cluster can be obtained from the volume of the object and a distribution of the number of cells existing as individual cells or clusters of various sizes produced. For cells not in direct contact, clustering can be quantified in terms of the number of neighbors within a given distance of each cell. In the case of T-cell antigen-recognition events where the APC is not fluorescently labeled, a cell to cell distance threshold of between 20 and 30 μm is appropriate.

When analyzing cell clustering, it is necessary to take into account that a certain number of apparent clusters can be expected by chance even in the case of totally independent cell motility. The likely number of such random clusters, which will increase with the number of cells in the imaging volume, can be estimated with simple Monte-Carlo simulations (Zinselmeyer *et al.*, 2005).

6.5. Analysis of cell migration

Once cells have been tracked and the raw data are in hand, several parameters can be used to quantitatively describe the migration behavior of the cells of interest.

6.5.1. Velocity

Cell velocity can be analyzed either as instantaneous velocity (Miller *et al.*, 2002) or track velocity (Aoshi *et al.*, 2008; Mempel *et al.*, 2004a; Zinselmeyer *et al.*, 2005). The most basic measure is ''instantaneous'' cell velocity, derived from the displacement of the cell centroid between adjacent time periods. Moreover, coarse time resolution between images can lead to an under estimate of peak cell velocities if cells velocities fluctuate rapidly. Because velocity can vary depending on the acquisition parameters.

The track velocity can be obtained as the median or mean instantaneous velocity computed from all time intervals throughout a track, typically 6 to 14 time points at 20- to 50-sec intervals. The instantaneously velocity can be easily computed for all cells within the imaging volume for pairs of adjacent time points, and the velocity distribution plotted as a histogram. Because some cells are very fast and transit the imaged area very quickly, it is difficult to track them so they are not included in the tracks, but they can still be a large part of the population; for this reason it makes sense to report instantaneous velocity (which is usually faster) as well as track velocity.

6.5.2. Displacement plot

The displacement from an initial position of an object moving with a constant velocity but randomly changing direction can be shown to be on average linearly proportional to the square root of the elapsed time (Wei *et al.*, 2003). A plot of mean displacement for a cell (or group of cells) vs time$^{1/2}$ (or more correctly displacement^2 vs time) provides an indication of whether cells are following random trajectories or are moving in a more directed fashion (neutrophil chemotaxis toward bacteria for instance). If cell movement is approximately a random walk, this plot yields a straight line on displacement^2 vs time, whereas directed motion will yield an upwardly curved plot. The linearity of the displacement plot can be estimated by fitting a straight line with linear regression and inspection of the goodness fit from the square of the correlation coefficient, R^2.

6.5.3. Motility coefficient

The slope of the fitted line on a displacement^2 vs time plot provides an estimate of the rate of random cell motion, with larger slopes indicating faster motion and greater displacement over any given period of time. By analogy with the diffusion coefficient of molecules, this has also been expressed as the 3-D motility coefficient Eq. (16.1) (Wei *et al.*, 2003).

$$D = \frac{slope^2}{6} \tag{16.1}$$

There is some confusion in the literature as to the correct form of the motility coefficient. The correct divisor is 4 if measurements were made only in 2D, and 6 if in 3D. The 'motility coefficient' should come out the same for both cases as cell motility is isotropic. In some cases, it may be simpler to report the slope of displacement vs time$^{1/2}$. For directed migration, a plot of displacement vs time with a similarly fitted straight line can be useful (Graham *et al.*, 2009).

6.5.4. Transit rate

For cells displaying a strong persistence of motion (i.e., continuing to move in the same direction), cell displacement from the origin over time (distance/time) is linear over long intervals. The slope of a linear regression line is equivalent to the cell interstitial transit rate. This descriptive parameter can be used to predict how long cells (e.g., neutrophils) will take to migrate from one location in the tissue (the blood vessels) to another area (site of bacterial infection). The transit rate is a robust parameter and can be compared between different experiments with different time settings as long as data for several positions of the same cell are available over a longer time interval (typically a minimum of 4 positions over 6 min). If cells are moving randomly, the motility coefficient is more appropriate to describe cell migration (see earlier). Both motility coefficient and transit rate can be compared even if calculated from samples with different acquisition times.

6.5.5. Arrest coefficient

This value is calculated as the ratio of the time cells are moving or not moving (instantaneous speeds $<2\ \mu m\ min^{1/2}$) vs the total time the cell is observed. The arrest coefficient is sensitive to the time interval of the experiment, because cell motility might be intermittent (i.e., with more frequent sampling, fewer arrested cells will be detected), and care must be taken to ensure that the sampling rate is the same when different groups are being compared. Considering that the arrest coefficient is calculated from cell tracks, the value reported will only represents a percentage of cells in the entire population.

6.5.6. Turning angle

The cell turning angle is the angular ($-180°$ to $+180°$) change in direction of cell motion within the plane defined by the locations of the cell within three successive images (Mempel *et al.*, 2004a). The distribution of turning angles provides an estimate of the directedness of cell motion. A cell exhibiting completely random motion would exhibit an even distribution of turning angles. Nonrandom or directed cell motion will show show an over abundance of prefered turning angles. Cell motility is influenced by turning angle and the instantaneous cell velocity, with motility being directly proportional to velocity and inversely proportional to turning angle. An example of a reduction in cell motility mediated by increased

turning angle rather than change in velocity can be seen in Mempel *et al.* (2004a). Finally, as for instantaneous velocity, the estimate of turning angle is very dependent on the image stack acquisition interval.

6.5.7. Meandering index

The meandering index for a cell track is computed as the displacement between the initial and final points on each the track divided by the total length of the random path. It provides another index of the directedness of cell movement. Cell movement in a straight line between the initial and final points, with no deviations, will yield a meandering index of 1. The more the track deviates from the straight line path, the lower the index value. Cells exhibiting frequent angle changes will produce tracks with lower meandering indices.

7. Presentation of 2P Microscopy Images

Presenting multidimensional data in an intelligible and convincing manner can be challenging, especially considering that our primary form of scientific communication is essentially a 2-D printed page.

7.1. 2-D images

The most common method for presenting 3-D z-stacks in 2-D is to create a maximum intensity projection (MIP) in the z-dimension. Maximum intensity projections can also be created along the x or y axis to show orthogonal views of 3-D–rendered images. The problem with this presentation method is that details are often obscured by fluorescence above or below the object of interest. A common solution is to show the z-stack as a sequence of images. Because individual z planes are shown, image details that were lost in the MIP are revealed and object colocalization can be easily confirmed in 3-D (x, y, and z or the thickness of the section).

An alternate method for presenting 3-D information on a 2-D page is to assign colors to different depths in the image, essentially color-encoding depth (Miller *et al.*, 2003). Z-sections or groups of z-sections are pseudo-colored blue, green, and red and slightly overlapped to create color scale that is useful for approximating a cell's position in 3-D space from a maximum intensity projection. This technique is limited by the number of colors available to encode the z-steps. However, it can be used to discriminate between colocalized cells and cells that are actually separated in the z-dimension but appear to be in contact because they overlap in the x- and y-dimensions.

It is important to include scale bars or measured grid lines and time stamps in the images whenever possible. This provides essential context for the reader and facilitates comparisons between different published studies. Most analysis programs contain dialogs for image contrast enhancement, color balancing, smoothing, and more. If used judiciously, image enhancement can help highlight key features of the image making them easier to interpret. However, there is always danger that overly manipulated images can obscure important details and bias the scientific interpretation. The best approach is that when image enhancement is required, use linear contrast enhancement methods (avoid manipulating the gamma) and standardize the process across experimental groups. As a general rule, it is best to present data with as little digital processing as possible.

Different smoothing algorithms can substantially affect the resulting image. If objects of interest are approximately spherical (e.g., an arrested lymphocyte), a Gaussian filter will work well to remove noise. On the other hand, if the object has more complex features, such as the fine processes of dendritic cells or collagen fibers, then a median filter will be better for enhancing the image without smoothing away important details. Most software programs have tutorials that will guide you through the process of selecting the proper filtering method for your images.

7.2. Cell tracks

Displaying cell tracks is a useful method for conveying qualitatively how a cell moves in the tissue. Cell tracks can be traced over a series of time-lapse images to show the paths of specific cells in the experiment. Individual cells can be shown with different colored lines, and points representing the cell's center of mass provide information about how fast the cell is moving and whether the movement is fluctuating or constant. Alternately, cell tracks can be normalized to their starting positions and overlaid on coordinate axes (Miller *et al.*, 2002). This presentation is especially useful for displaying random cell migration. The reader can see quickly multiple representative cell tracks and gain a sense of whether the paths are straight, curved, disjointed, or a heterogeneous mixture. This same plot can suggest that cell migration is constrained or has a directional bias. Okada *et al.* (2005) used cell track plots from different regions to show that the migration of antigen-specific B cells changed from random to highly directed (consistent with chemotaxis) near the follicular boundary.

7.3. 3-D rotations and time-lapse movies

Presenting multidimensional data has become easier as many journals now host supplemental movies on their web sites to support published work. In general, it is useful to start with a written description of the phenomena accompanied by a supplemental movie so that the reader has an opportunity to grasp the overall 3-D structure or behavior of interest. Popular formats include QuickTime and AVI, which strike a good balance between the need for sufficient resolution with the need for the file to be small enough for download from a web site. We typically smooth and contrast-enhance the movies to bring out the elements of interest. This should not be done on the primary data (this could affect the analysis), but on a duplicate data set used only for presentation purposes. Annotations such as a scale bar and time stamp are highly recommended. If possible, identify the cell or behavior of interest by circling or placing arrows in the movie. The more annotation the movie has the easier it is for the reader to understand what you are attempting to show. Figure captions should give details about the time and spatial resolution of the images and general information regarding any digital enhancements that were made.

REFERENCES

Aoshi, T., Zinselmeyer, B. H., Konjufca, V., Lynch, J. N., Zhang, X., Koide, Y., and Miller, M. J. (2008). Bacterial entry to the splenic white pulp initiates antigen presentation to $CD8^+$ T cells. *Immunity* **29,** 476–486.

Beuneu, H., Garcia, Z., and Bousso, P. (2006). Cutting edge: Cognate CD4 help promotes recruitment of antigen-specific CD8 T cells around dendritic cells. *J. Immunol.* **177,** 1406–1410.

Bhakta, N. R., and Lewis, R. S. (2005). Real-time measurement of signaling and motility during T cell development in the thymus. *Semin. Immunol.* **17,** 411–420.

Bhakta, N. R., Oh, D. Y., and Lewis, R. S. (2005). Calcium oscillations regulate thymocyte motility during positive selection in the three-dimensional thymic environment. *Nat. Immunol.* **6,** 143–151.

Boissonnas, A., Fetler, L., Zeelenberg, I. S., Hugues, S., and Amigorena, S. (2007). *In vivo* imaging of cytotoxic T cell infiltration and elimination of a solid tumor. *J. Exp. Med.* **204,** 345–356.

Bousso, P., and Robey, E. A. (2004). Dynamic behavior of T cells and thymocytes in lymphoid organs as revealed by two-photon microscopy. *Immunity* **21,** 349–355.

Castellino, F., Huang, A. Y., Altan-Bonnet, G., Stoll, S., Scheinecker, C., and Germain, R. N. (2006). Chemokines enhance immunity by guiding naive CD8(+) T cells to sites of CD4 T cell-dendritic cell interaction. *Nature* **440,** 890–895.

Cavanagh, L. L., Bonasio, R., Mazo, I. B., Halin, C., Cheng, G. Y., van der Velden, A. W. M., Cariappa, A., Chase, C., Russell, P., Starnbach, M. N., Koni, P. A., Pillai, S., Weninger, W., and von Andrian, U. H. (2005). Activation of bone marrow-resident memory T cells by circulating, antigen-bearing dendritic cells. *Nat. Immunol.* **6,** 1029–1037.

Celso, C. L., Fleming, H. E., Wu, J. W., Zhao, C. X., Miake-Lye, S., Fujisaki, J., Cote, D., Rowe, D. W., Lin, C. P., and Scadden, D. T. (2008). Live-animal tracking of individual haematopoietic stem/progenitor cells in their niche. *Nature* **457,** 92–96.

Chieppa, M., Rescigno, M., Huang, A. Y., and Germain, R. N. (2006). Dynamic imaging of dendritic cell extension into the small bowel lumen in response to epithelial cell TLR engagement. *J. Exp. Med.* **203,** 2841–2852.

Denk, W., Strickler, J. H., and Webb, W. W. (1990). 2-Photon laser scanning fluorescence microscopy. *Science* **248,** 73–76.

Egen, J. G., Rothfuchs, A. G., Feng, C. G., Winter, N., Sher, A., and Germain, R. N. (2008). Macrophage and T cell dynamics during the development and disintegration of mycobacterial granulomas. *Immunity* **28,** 271–284.

Faust, N., Varas, F., Kelly, L. M., Heck, S., and Graf, T. (2000). Insertion of enhanced green fluorescent protein into the lysozyme gene creates mice with green fluorescent granulocytes and macrophages. *Blood* **96,** 719–726.

Fork, R. L. (1986). Optical frequency filter for ultrashort pulses. *Opt. Lett.* **11,** 629–631.

Gauderon, R., Lukins, P. B., and Sheppard, C. J. (2001). Simultaneous multichannel nonlinear imaging: Combined two-photon excited fluorescence and second-harmonic generation microscopy. *Micron* **32,** 685–689.

Geissmann, F., Jung, S., and Littman, D. R. (2003). Blood monocytes consist of two principal subsets with distinct migratory properties. *Immunity* **19,** 71–82.

Gelman, A. E., Li, W., Richardson, S. B., Zinselmeyer, B. H., Lai, J., Okazaki, M., *et al.* (2009). Cutting edge: Acute lung allograft rejection is independent of secondary lymphoid organs. *J. Immunol.* **182,** 3969–3973.

Germain, R. N., Castellino, F., Chieppa, M. C., Egen, J. G., Huang, A. Y. C., Koo, L. Y., and Hai, Q. (2005). An extended vision for dynamic high-resolution intravital immune imaging. *Semin. Immunol.* **17,** 431–441.

Germain, R. N., Miller, M. J., Dustin, M. L., and Nussenzweig, M. C. (2006). Dynamic imaging of the immune system: Progress, pitfalls and promise. *Nat. Rev. Immunol.* **6,** 497–507.

Graham, D. B., Zinselmeyer, B. H., Mascarenhas, F., Delgado, R., Miller, M. J., and Swat, W. (2009). ITAM signaling by Vav family Rho guanine nucleotide exchange factors regulates interstitial transit rates of neutrophils *in vivo*. *PLoS ONE* **4,** e4652.

Göppert, M. (1929). Über die Wahrscheinlichkeit des Zusammenwirkens zweier Lichtquanten in einem Elementarakt. *Naturwissenschaften.* **17,** 932–932.

Huang, J. H., Cardenas-Navia, L. I., Caldwell, C. C., Plumb, T. J., Radu, C. G., Rocha, P. N., Wilder, T., Bromberg, J. S., Cronstein, B. N., Sitkovsky, M., Dewhirst, M. W., and Dustin, M. L. (2007). Requirements for T lymphocyte migration in explanted lymph nodes. *J. Immunol.* **178,** 7747–7755.

Hugues, S., Boissonnas, A., Amigorena, S., and Fetler, L. (2006). The dynamics of dendritic cell-T cell interactions in priming and tolerance. *Curr. Opin. Immunol.* **18,** 491–495.

Kawakami, N., Nagerl, U. V., Odoardi, F., Bonhoeffer, T., Wekerle, H., and Flugel, A. (2005). Live imaging of effector cell trafficking and autoantigen recognition within the unfolding autoimmune encephalomyelitis lesion. *J. Exp. Med.* **201,** 1805–1814.

Lammermann, T., Bader, B. L., Monkley, S. J., Worbs, T., Wedlich-Soldner, R., Hirsch, K., Keller, M., Forster, R., Critchley, D. R., Fassler, R., and Sixt, M. (2008). Rapid leukocyte migration by integrin-independent flowing and squeezing. *Nature* **453,** 51–55.

Lee, G. S., Miele, L. F., Turhan, A., Lin, M., Hanidziar, D., Konerding, M. A., and Mentzer, S. J. (2008). Spatial calibration of structured illumination fluorescence microscopy using capillary tissue phantoms. *Microsc. Res. Tech.* **72,** 85–92.

Leybaert, L., de Meyer, A., Mabilde, C., and Sanderson, M. J. (2005). A simple and practical method to acquire geometrically correct images with resonant scanning-based line

scanning in a custom-built video-rate laser scanning microscope. *J. Microsc.* **219,** 133–140.

Lindquist, R. L., Shakhar, G., Dudziak, D., Wardemann, H., Eisenreich, T., Dustin, M. L., and Nussenzweig, M. C. (2004). Visualizing dendritic cell networks *in vivo*. *Nat. Immunol.* **5,** 1243–1250.

Masters, B. R., and So, P. T. C. (2008). "Handbook of Biomedical Nonlinear Optical Microscopy. Oxford: Oxford University Press.

Matheu, M. P., Beeton, C., Garcia, A., Chi, V., Rangaraju, S., Safrina, O., Monaghan, K., Uemura, M. I., Li, D., Pal, S., de la Maza, L. M., Monuki, E., Flugel, A., Pennington, M. W., Parker, I., Chandy, K. G., and Cahalan, M. D. (2008a). Imaging of effector memory T cells during a delayed-type hypersensitivity reaction and suppression by Kv1.3 channel block. *Immunity* **29,** 602–614.

Matheu, M. P., Beeton, C., Parker, I., and Chandy, K. G. (2008b). Imaging effector memory T cells in the ear after induction of adoptive DTH. *J. Vis. Exp.*

Matheu, M. P., and Cahalan, M. D. (2007). Isolation of $CD4^+$ T cells from mouse lymph nodes using Miltenyi MACS purification. *J. Vis. Exp.* **409**.

Matheu, M. P., Parker, I., and Cahalan, M. D. (2007). Dissection and 2-photon imaging of peripheral lymph nodes in mice. *J. Vis. Exp.* **265**.

Mempel, T. R., Henrickson, S. E., and von Andrian, U. H. (2004a). T-cell priming by dendritic cells in lymph nodes occurs in three distinct phases. *Nature* **427,** 154–159.

Mempel, T. R., Pittet, M. J., Khazaie, K., Weninger, W., Weissleder, R., von Boehmer, H., and von Andrian, U. H. (2006). Regulatory T cells reversibly suppress cytotoxic T cell function independent of effector differentiation. *Immunity* **25,** 129–141.

Mempel, T. R., Scimone, M. L., Mora, J. R., and von Andrian, U. H. (2004b). *In vivo* imaging of leukocyte trafficking in blood vessels and tissues. *Curr. Opin. Immunol.* **16,** 406–417.

Miller, M. J., Hejazi, A. S., Wei, S. H., Cahalan, M. D., and Parker, I. (2004a). T cell repertoire scanning is promoted by dynamic dendritic cell behavior and random T cell motility in the lymph node. *Proc. Natl. Acad. Sci. USA* **101,** 998–1003.

Miller, M. J., Safrina, O., Parker, I., and Cahalan, M. D. (2004b). Imaging the single cell dynamics of CD4(+) T cell activation by dendritic cells in lymph nodes. *J. Exp. Med.* **200,** 847–856.

Miller, M. J., Wei, S. H., Cahalan, M. D., and Parker, I. (2003). Autonomous T cell trafficking examined in vivo with intravital two-photon microscopy. *Proc. Natl. Acad. Sci. USA* **100,** 2604–2609.

Miller, M. J., Wei, S. H., Parker, I., and Cahalan, M. D. (2002). Two-photon imaging of lymphocyte motility and antigen response in intact lymph node. *Science* **296,** 1869–1873.

Millington, O. R., Zinselmeyer, B. H., Brewer, J. M., Garside, P., and Rush, C. M. (2007). Lymphocyte tracking and interactions in secondary lymphoid organs. *Inflamm. Res.* **56,** 391–401.

Nguyen, Q. T., Callamaras, N., Hsieh, C., and Parker, I. (2001). Construction of a two-photon microscope for video-rate Ca2+ imaging. *Cell Calcium* **30,** 383–393.

Okada, T., Miller, M. J., Parker, I., Krummel, M. F., Neighbors, M., Hartley, S. B., O'Garra, A., Cahalan, M. D., and Cyster, J. G. (2005). Antigen-engaged B cells undergo chemotaxis toward the T zone and form motile conjugates with helper T cells. *Plos Biol.* **3,** 1047–1061.

Peters, N. C., Egen, J. G., Secundino, N., Debrabant, A., Kimblin, N., Kamhawi, S., Lawyer, P., Fay, M. P., Germain, R. N., and Sacks, D. (2008). *In vivo* imaging reveals an essential role for neutrophils in leishmaniasis transmitted by sand flies. *Science* **321,** 970–974.

Rocheleau, J. V., and Piston, D. W. (2003). Two-photon excitation microscopy for the study of living cells and tissues. *Curr. Protoc. Cell Biol.* **4,** Unit 4 11.

Rothstein, E. C., Carroll, S., Combs, C. A., Jobsis, P. D., and Balaban, R. S. (2005). Skeletal muscle NAD(P)H two-photon fluorescence microscopy *in vivo*: Topology and optical inner filters. *Biophys. J.* **88,** 2165–2176.

Shakhar, G., Lindquist, R. L., Skokos, D., Dudziak, D., Huang, J. H., Nussenzweig, M. C., and Dustin, M. L. (2005). Stable T cell-dendritic cell interactions precede the development of both tolerance and immunity *in vivo*. *Nat. Immunol.* **6,** 707–714.

Tang, Q. Z., Adams, J. Y., Tooley, A. J., Bi, M. Y., Fife, B. T., Serra, P., Santamaria, P., Locksley, R. M., Krummel, M. F., and Bluestone, J. A. (2006). Visualizing regulatory T cell control of autoimmune responses in nonobese diabetic mice. *Nat. Immunol.* **7,** 83–92.

Vintersten, K., Monetti, C., Gertsenstein, M., Zhang, P., Laszlo, L., Biechele, S., and Nagy, A. (2004). Mouse in red: Red fluorescent protein expression in mouse ES cells, embryos, and adult animals. *Genesis* **40,** 241–246.

von Andrian, U. H. (2002). Immunology. T cell activation in six dimensions. *Science* **296,** 1815–1817.

Wei, S. H., Parker, I., Miller, M. J., and Cahalan, M. D. (2003). A stochastic view of lymphocyte motility and trafficking within the lymph node. *Immunol. Rev.* **195,** 136–159.

White, J. G., Amos, W. B., and Fordham, M. (1987). An evaluation of confocal versus conventional imaging of biological structures by fluorescence light microscopy. *J. Cell Biol.* **105,** 41–48.

Witt, C. M., Raychaudhuri, S., Schaefer, B., Chakraborty, A. K., and Robey, E. A. (2005). Directed migration of positively selected thymocytes visualized in real time. *Plos Biol.* **3,** 1062–1069.

Wokosin, D. L., Loughrey, C. M., and Smith, G. L. (2004). Characterization of a range of fura dyes with two-photon excitation. *Biophys. J.* **86,** 1726–1738.

Yeh, A. T., Nassif, N., Zoumi, A., and Tromberg, B. J. (2002). Selective corneal imaging using combined second-harmonic generation and two-photon excited fluorescence. *Opt. Lett.* **27,** 2082–2084.

Yuste, R., Konnerth, A., and Cold Spring Harbor, L. (2005). "Imaging in Neuroscience and Development: A Laboratory Manual. Cold Spring Harbor, NY: Cold Spring Harbor Laboratory Press.

Zinselmeyer, B. H., Dempster, J., Gurney, A. M., Wokosin, D., Miller, M., Ho, H., Millington, O. R., Smith, K. M., Rush, C. M., Parker, I., Cahalan, M., Brewer, J. M., and Garside, P. (2005). *In situ* characterization of CD4(+) T cell behavior in mucosal and systemic lymphoid tissues during the induction of oral priming and tolerance. *J. Exp. Med.* **201,** 1815–1823.

Zinselmeyer, B. H., Lynch, J. N., Zhang, X., Aoshi, T., and Miller, M. J. (2008). Video-rate two-photon imaging of mouse footpadA promising model for studying leukocyte recruitment dynamics during inflammation. *Inflamm. Res.*

Zoumi, A., Yeh, A., and Tromberg, B. J. (2002). Imaging cells and extracellular matrix *in vivo* by using second-harmonic generation and two-photon excited fluorescence. *Proc. Natl. Acad. Sci. USA* **99,** 11014–11019.